

# HGARN: Hierarchical Graph Attention Recurrent Network for Human Mobility Prediction

Yihong Tang  
University of Hong Kong  
yihongt@connect.hku.hk

Junlin He  
Beijing University of Posts and  
Telecommunications  
mr.h@bupt.edu.cn

Zhan Zhao\*  
University of Hong Kong  
zhanzhao@hku.hk

## ABSTRACT

Human mobility prediction is a fundamental task essential for various applications, including urban planning, transportation services, and location recommendation. Existing approaches often ignore activity information crucial for reasoning human preferences and routines, or adopt a simplified representation of the dependencies between time, activities and locations. To address these issues, we present *Hierarchical Graph Attention Recurrent Network (HGARN)* for human mobility prediction. Specifically, we construct a hierarchical graph based on all users' history mobility records and employ a *Hierarchical Graph Attention Module* to capture complex time-activity-location dependencies. This way, HGARN can learn representations with rich contextual semantics to model user preferences at the global level. We also propose a model-agnostic history-enhanced confidence (MAHEC) label to focus our model on each user's individual-level preferences. Finally, we introduce a *Recurrent Encoder-Decoder Module*, which employs recurrent structures to jointly predict users' next activities (as an auxiliary task) and locations. For model evaluation, we test the performances of our HGARN against existing SOTAs in *recurring* and *explorative* settings<sup>1</sup>. The *recurring* setting focuses more on assessing models' capabilities to capture users' individual-level preferences. In contrast, the results in the *explorative* setting tend to reflect the power of different models to learn users' global-level preferences. Overall, our model outperforms other baselines significantly in the main, *recurring*, and *explorative* settings based on two real-world human mobility data benchmarks. Source codes of HGARN are available at <https://github.com/YihongT/HGARN>.

## KEYWORDS

Human Mobility, Next Location Prediction, Hierarchical Graph

## INTRODUCTION

Human mobility is critical for various downstream applications such as urban planning, transportation services, location recommendation, and epidemic management. The ability to model and accurately predict future human mobility can inform us about important public policy decisions for society's betterment, such as promoting social integration, encouraging innovation, and maximizing productivity [29]. Central to human mobility modeling is the problem of next location prediction, i.e., the prediction of where an individual is going next, which has received great attention. On the one hand, the increasing prevalence of mobile devices and the popularity of location-based social networks (LBSNs) provide

\*Corresponding author.

<sup>1</sup>*Recurring* indicates a user's next location was visited before, whereas *Explorative* indicates a user's next location was not visited in the history mobility, see Figure A3.

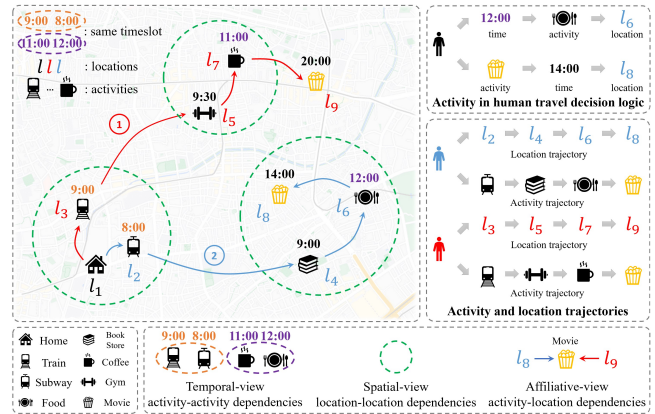


**Figure 1: An illustration of two human mobility trajectories. Activities are essential in affecting human travel decisions and in modeling multiple dependencies.**

unprecedented data sources for mining individual-level mobility traces and preferences [38]. On the other hand, the advancement of AI and machine learning offers a plethora of analytical tools for modeling human mobility. These innovations have supercharged the development of human mobility models in the past decade, especially for the next location prediction.

Traditional approaches studied human mobility over sequential transitions, where several approaches explored using Markov Chains (Mc) [10, 25, 28] to model transition patterns over location sequences. Later, recurrent neural network-based [13] models demonstrated better predictive power over Mc-based methods, where pioneering works employed recurrent structures to model temporal periodicity [9] and spatial regularity [36]. Some other RNN-based methods incorporate spatial and temporal contexts [21, 30] into the RNN update process to boost models' performances. In addition, due to the great success of the TRANSFORMER architecture [31], the attention mechanism has also been adopted in several works [12, 22] to better model sequences and obtain good prediction results. In recent years, graph-based approaches leveraged graph representation learning [3, 37] and graph neural networks (GNNs) [15] to model user preferences [20] and the spatial-temporal relationships [8, 22] between locations, obtaining rich representations [27, 33] to improve the performance of the next location prediction. While these works rely on mining individual location sequences for human mobility prediction, they rarely consider the underlying travel behavior structure and activity information. In the travel behavior literature, an individual's decision to visit a location is

usually considered to be derived from their daily activity patterns [2]. As a result, important inter-dependencies exist between activity participation and location visitation behaviors, which are often overlooked. Furthermore, the number of possible activity categories is much smaller than the number of locations, making it easier to obtain a robust estimate for the former. With data regarding human activity patterns becoming increasingly accessible, it is both behaviorally meaningful and computationally efficient to incorporate such activity information and its spatial-temporal dependencies in human mobility modeling.

Figure 1 shows a couple of human mobility trajectories reflecting time-activity-location dependencies. For example, when the time is approaching noon, one user may decide to dine at a nearby restaurant, and another may go to the movie theater for a specific starting time. These examples illustrate that activities are usually scheduled according to the time of day, affecting the choice of which location to visit next, as also evidenced by Figure A4, where people usually go to restaurants at noon and mostly return home or go to the gym at night. However, only a few works have considered adding activity information (e.g., location categories) to improve next location prediction. Yu et al. [39] used activities along with spatial distances to reduce search space (i.e., candidate locations). Huang et al. [14] proposed a CSLSL which comprises an RNN-based [7] structure, where the time, activity, and location are predicted sequentially to model human travel decision logic. However, the design of CSLSL oversimplifies the time-activity-location dependencies. Given data sparsity and behavioral uncertainties [44], the time prediction tends to be more challenging [43], which can further compromise the prediction of activities and locations.

To the best of our knowledge, no efforts have been made to model the sophisticated time-activity-location dependencies and leverage them to improve the next location prediction. In this paper, we present *Hierarchical Graph Attention Recurrent Network (HGARN)* for the next location prediction. Specifically, we first construct a hierarchical graph based on time-activity-location history mobility records of all users and employ a *Hierarchical Graph Attention Module* to capture complex temporal-view activity-activity, affiliated-view activity-location, spatial-view location-location dependencies. In this way, HGARN can learn representations with rich contextual semantics to model user preferences at the global level. Correspondingly, a model-agnostic history-enhanced confidence (MAHEC) label is proposed to guide our model to learn each user’s individual-level preferences. We finally introduce a *Recurrent Encoder-Decoder Module*. The module takes the sequence of user embeddings combined with the learned hierarchical graph representations as input to jointly predict a user’s next activity (as the auxiliary task) and location (as the main task). Specifically, the former can be residually incorporated into the latter. In such a design, our model can leverage the learned time-activity-location dependencies to benefit both global- and individual-level human mobility modeling, and use predicted next activity distribution to facilitate model performance for personalized next location prediction.

In summary, our paper makes the following contributions:

- We propose a Hierarchical Graph to represent the temporal-view activity-activity, affiliated-view activity-location, spatial-view location-location dependencies. To the best of our knowledge,

among the few approaches incorporating activity information into the next location prediction, this is the first work to model the dependencies of time, activities and locations by leveraging a Hierarchical Graph.

- We design a Hierarchical Graph Attention Recurrent Network (i.e., HGARN), which contains a *hierarchical graph attention module* to model dependencies between time, activities, and locations to capture users’ global-level preferences, and a *recurrent encoder-decoder module* to incorporate the hierarchical graph representations into sequence modeling and utilize next activity prediction to boost the next location prediction.
- We introduce a simple yet effective model-agnostic history-enhanced confidence (MAHEC) label to guide our model to learning each user’s individual-level preferences, which enables the model to focus more on relevant locations in their history trajectories when predicting their next locations.
- Extensive experiments are conducted using two real-world location-based social networks (LBSN) check-in datasets. Specifically, we evaluate the prediction performance of our HGARN against existing SOTAs in the main, *recurring*, and *explorative* settings. Our work is the first to separately evaluate the next location prediction models’ *recurring* and *explorative* prediction performances. The results show that the HGARN can significantly outperform existing methods in all experimental settings.

## RELATED WORK

The next location prediction is essentially about sequence modeling since successive location visits are usually correlated [5, 40]. Traditional MC-based methods often incorporate other techniques, such as matrix factorization [28] and activity-based modeling [25] to capture mobility patterns and make predictions. However, MC-based methods are limited in capturing long-term dependencies or predicting *explorative* human mobility.

Deep learning-based approaches consider the next location prediction a sequence-to-sequence task and obtain better prediction results than traditional methods. The majority of existing deep models are based on Recurrent neural networks [6, 13] (RNN). STRNN [21] is a pioneering work that incorporates spatial-temporal features between consecutive human visits into RNN models to predict human mobility. STGN [42] adds spatial and temporal gates to LSTM to learn users’ interests. FLASHBACK [36] leverages spatial and temporal intervals to compute an aggregated past RNN hidden states for predictions. LSTPM [30] introduces a non-local network and a geo-dilated LSTM to model users’ long- and short-term preferences. Some approaches use the attention mechanism to improve their performances. DEEPMOVE [9] leveraged attention mechanisms combined with an RNN module to capture users’ long- and short-term preferences. ARNN [12] uses a knowledge graph to find related neighbor locations and model the sequential regularity of check-ins through attentional RNN. STAN [22] extracts relative spatial-temporal information between consecutive and non-consecutive locations through a spatio-temporal attention network for locations predictions. In addition, some efforts incorporate contextual information [17] such as geographical information [18], dynamic-static [24], text content about locations [4] into sequence modeling.

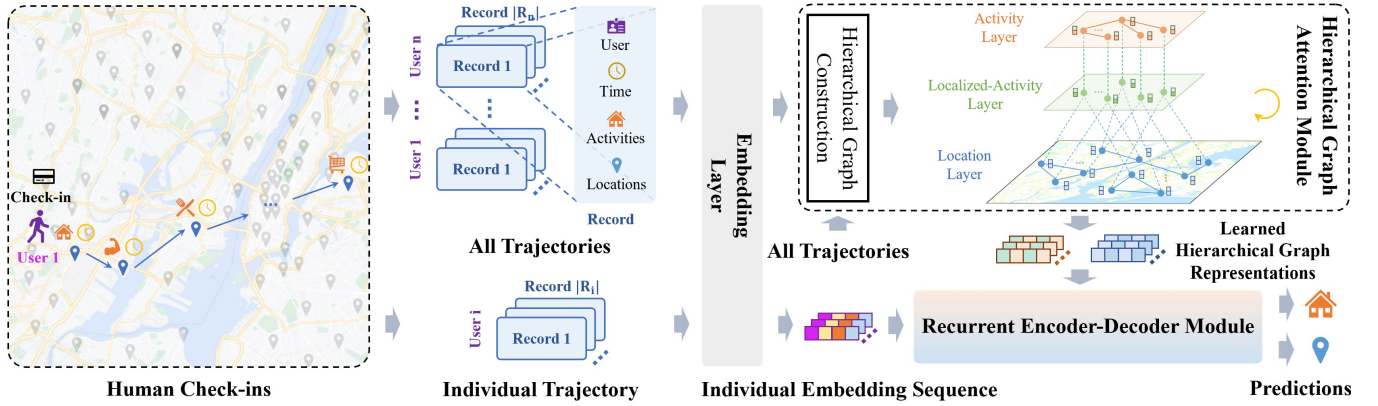


Figure 2: A workflow of the proposed HGARN.

Recently, graph-based models have been designed to enrich contextual features, which can reflect global preferences. LBSN2VEC [37] performs random walks on a hypergraph to learn embeddings for next location and friendship predictions. STP-UDGAT [20] uses GAT to learn location relationships from both local and global views based on constructed spatial, temporal, and preference graphs. HMT-GRN [19] learned several user-region matrices of different granularity levels to alleviate the data sparsity issue and efficiently predict next locations. GCDAN [8] uses dual attention to model the high-order sequential dependencies and graph convolutions to mitigate the data sparsity issue. GRAPH-FLASHBACK [27] uses knowledge graph embedding to construct transition graph, and applies GCN to refine graph representations and combines with FLASHBACK to make predictions.

Some other works focused on different aspects, activity-aware methods like [1] model the activities with a weighted category hierarchy (WCH), CATDM [39] uses activities along with spatial distances to reduce search space, CSLSL [14] proposed an RNN-based causal structure to capture human travel decision logic. However, most existing methods ignore activity information and cannot effectively model the time-activity-location dependencies, which are essential for predicting and understanding human mobility.

## PRELIMINARIES

This section introduces definitions relevant to this study and then formulates the next location prediction problem.

We use notations  $U = \{u^i\}_{i=1}^{|U|}$ ,  $L = \{l^i\}_{i=1}^{|L|}$ ,  $C = \{c^i\}_{i=1}^{|C|}$ , and  $T = \{t^i\}_{i=1}^{|T|}$  to denote the sets of users, locations, activities and time series, respectively. In particular, we denote a user  $u \in U$ 's sets of locations, activities and time series in a temporal order as  $L_u = \{l_u^i\}_{i=1}^{|L_u|}$ ,  $C_u = \{c_u^i\}_{i=1}^{|C_u|}$ , and  $T_u = \{t_u^i\}_{i=1}^{|T_u|}$ , where  $\delta_u^i$  may not equal to  $\delta^i$ ,  $\delta \in \{U, L, C, T\}$ .

**DEFINITION 1 (MOBILITY RECORD).** We use the notation  $r$  to denote a single human mobility record. Specifically, the  $i$ th record of a given user  $u \in U$  is represented by a tuple  $r_u^i = (u, c_u^i, l_u^i, t_u^i)$ . Each record tuple comprises a user  $u \in U$ , an activity  $c_u^i \in C_u$ , a location  $l_u^i \in L_u$  and the visit time  $t_u^i \in T_u$ .

**DEFINITION 2 (TRAJECTORY).** A trajectory is a sequence of mobility records that belongs to a user  $u \in U$ , denoted by  $R_u = \{r_u^i\}_{i=1}^{|R_u|}$ . Each trajectory  $R_u$  can be divided into a history trajectory  $R_u^{his} = \{r_u^i\}_{i=1}^{|R_u|-1}$  and the final record  $r_u^{|R_u|}$ . In this way, we can obtain the user  $u$ 's activity trajectories  $R_u^C = \{c_u^i\}_{i=1}^{|R_u|}$ , location trajectories  $R_u^L = \{l_u^i\}_{i=1}^{|R_u|}$ , and time trajectories  $R_u^T = \{t_u^i\}_{i=1}^{|R_u|}$  with their history trajectories  $R_u^{C,his}$ ,  $R_u^{L,his}$  and  $R_u^{T,his}$ .

Given the definitions above, the next location prediction problem can be formulated as follows:

**PROBLEM 1 (NEXT LOCATION PREDICTION).** Given a user  $u \in U$ 's history trajectory  $R_u^{his}$  as input, we consider  $u$ 's next record as its future state. The human mobility prediction task  $\mathcal{T}$  maps  $u$ 's history trajectory  $R_u^{his}$  to  $u$ 's next location  $l_u^{|R_u|}$  in the future. The above-described process can be summarized as follows:

$$R_u^{his} \xrightarrow{\mathcal{T}(\cdot; \theta)} l_u^{|R_u|}, \quad (1)$$

where  $\theta$  is the parameters of mapping  $\mathcal{T}$ .

## METHODOLOGY

The HGARN's workflow is demonstrated in Figure 2. The raw data is first encoded in the *embedding layer* and then input to the *hierarchical graph attention module* to model multi-dependencies. Finally, the user's personalized embeddings are fused with the learned hierarchical graph representations and input to the *recurrent encoder-decoder module* to make predictions. In the following sections, we will elaborate on the details of our HGARN.

### Embedding Layer

We first introduce our *embedding layer*, which aims to assign trainable embeddings to each unique mobility record element, i.e., the user, activity, location and time. It is worth noting that all these elements are discrete values except for time, and it is necessary to split the continuous time into discrete intervals to facilitate the encoding of time. In this work we discretize the 24 hours of the day into  $|T^h|$  time slots  $T^h = \{h\}_{h=1}^{|T^h|}$  and another variable  $T^w = \{w\}_{w=1}^{|T^w|}$  indicating the day of the week. Note that all  $t \in T$  can be written in the

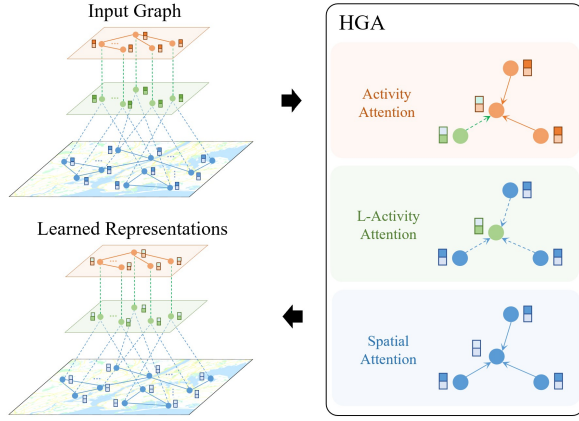


Figure 3: The design of *hierarchical graph attention module*.

form of  $t = (h, w)$ . We obtain the embeddings of each user, activity, location and time  $e_u \in \mathbb{R}^{d^u}$ ,  $e_c, e_l \in \mathbb{R}^d$ ,  $e_t \in \mathbb{R}^{d^t}$  by multiplying their one-hot vectors with the corresponding trainable transformation matrices, where  $d^u, d$  and  $d^t$  represent embedding dimensions.  $e_U \in \mathbb{R}^{|U| \times d^u}$ ,  $e_C \in \mathbb{R}^{|C| \times d}$ ,  $e_L \in \mathbb{R}^{|L| \times d}$  and  $e_T \in \mathbb{R}^{|T| \times d^t}$  are used to denote the embedding matrices for the user, activity, location and time, respectively.  $e_{r_u^i} = (e_u, e_{c_u^i}, e_{l_u^i}, e_{t_u^i})$  is used to denote a user  $u$ 's embeddings of  $i$ th record.

### Hierarchical Graph Attention Module

The *hierarchical graph attention module* consists of two parts: hierarchical graph construction and hierarchical graph attention (HGA) networks on the graph for multi-dependencies modeling.

*Hierarchical Graph Construction.* Given that a spatial network is naturally a graph and recent advances in graph neural networks [23, 32], we choose to model the location-location, location-activity and activity-activity dependencies with a hierarchical graph.

The constructed hierarchical graph is shown in Figure 3, which includes three layers: location layer, localized-activity layer, and activity layer, where the localized-activity layer is adopted to suppress noise aggregated from the location layer. We formally describe the hierarchical graph with notation  $G = (V, E)$ , where  $V = V^L \cup V^C \cup V^{C'}$  and  $E = \{A^L, A^C, A^{LC'}, A^{CC'}\}$ . Specifically,  $V^L$  and  $V^C$  represents the location node-set and the activity node-set.  $V^{C'}$  indicates the localized-activity node-set.  $E$  comprises four adjacency matrices that denote connectivity between (1) two location nodes, (2) two activity nodes, (3) a location node and a localized-activity node, (4) an activity node and a localized-activity node.

For the location adjacency matrix  $A^L$ , we utilize the geographical distance to determine whether two nodes are linked. We employ the *haversine formula* to compute distances between locations. Given  $l^i$  and  $l^j$  and their GPS data,  $A^L \in \mathbb{R}^{|L| \times |L|}$  is as:

$$A_{l^i, l^j}^L = \begin{cases} 1, & \text{Haversine}(\text{GPS}^i, \text{GPS}^j) < D^h \\ 0, & \text{otherwise} \end{cases}, \quad (2)$$

where  $D^h$  is a hyperparameter to control the distance threshold to influence the connectivity between locations.

The construction of  $A^C$  is based on history trajectories of all users. Intuitively, the dependency between two activities can be measured by the frequency of co-occurrence in the same time interval  $h \in T^h$ . However, if we directly consider the activity co-occurrence frequency based on all trajectories (regardless of the user), it may lead to unrelated activities being interrelated (e.g., check-in at subway stations and gyms both often occur in the evening), due to the difference in user preferences. Instead, a more reasonable way is to learn the inter-activity dependencies based on activity co-occurrence within individual-level trajectory sets. Therefore, we can traverse the history trajectories of each user  $u \in U$  and calculate the co-occurrence matrix  $M^C \in \mathbb{R}^{|C| \times |C|}$ :

$$M_{c_u^i, c_u^j}^C = \sum_{u \in U} \sum_{i=1}^{|R_u^{\text{his}}|} \sum_{j=i+1}^{|R_u^{\text{his}}|} \mathbf{1}_h(h_u^i, h_u^j), \quad (3)$$

$$\mathbf{1}_h(h_u^i, h_u^j) = \begin{cases} 1, & \text{if } h_u^i = h_u^j \\ 0, & \text{otherwise} \end{cases}, \quad (4)$$

where  $\mathbf{1}_h(\cdot)$  is an indicator function. Larger elements in the  $M^C$  indicate stronger dependencies between the corresponding two activities. For the sake of simplicity and suppression of correlation between some of the less relevant activities, we calculate the adjacency between each activity pair  $(c^i, c^j)$  to attain  $A^C \in \mathbb{R}^{|C| \times |C|}$ :

$$A_{c^i, c^j}^C = \begin{cases} 1, & \text{if } M_{c^i, c^j}^C > \text{mean}(M^C) \\ 0, & \text{otherwise} \end{cases}, \quad (5)$$

The matrix  $A^{LC'}$  defines the adjacency between nodes of the location layer and nodes of the localized-activity layer. Each node of  $V^L$  is linked to only one node of  $V^{C'}$ , representing the corresponding activity category at that location. In contrast, each node of  $V^{C'}$  may be linked to multiple nodes of  $V^L$ , as several locations can share the same activity. Formally, we define  $A_L^{LC'} \in \mathbb{R}^{|L| \times |C|}$  based on the affiliations of locations and activities, where each row corresponds to a location and each column an activity. Additionally, we construct the adjacency matrix  $A^{LC'} \in \mathbb{R}^{(|L|+|C|) \times (|L|+|C|)}$  based on  $A_L^{LC'}$  in the following block matrix form:

$$A^{LC'} = \begin{bmatrix} O_L & A_L^{LC'} \\ (A_L^{LC'})^\top & O_C \end{bmatrix}, \quad (6)$$

where  $(A^{LC'})^\top$  is the transpose of  $A^{LC'}$ ,  $O_L \in \mathbb{R}^{|L| \times |L|}$  and  $O_C \in \mathbb{R}^{|C| \times |C|}$  are two zero matrices.

The function of the localized-activity layer is to suppress noise from the location layer aggregated to the activity layer, so we simply define that each node in the localized-activity layer is connected to the node in the activity layer representing the same activity. Mathematically, similar to Equation 6, we have  $A^{CC'} \in \mathbb{R}^{2|C| \times 2|C|}$ :

$$A^{CC'} = \begin{bmatrix} O_C & I_C \\ I_C & O_C \end{bmatrix}, \quad (7)$$

where  $I_C \in \mathbb{R}^{|C| \times |C|}$  is an identity matrix.

*Hierarchical Graph Attention Networks.* Inspired by recent work conducted deep learning on hierarchical graphs [11, 34, 41], we design a hierarchical graph attention network (HGA) to model the hierarchical graph we just defined. Since the importance of locations

within a certain distance is different for a specific location, we employ graph attention mechanisms to model spatial-view location-location dependencies:

$$H^L = \text{GAT}_L(e_L, A^L), \quad (8)$$

where  $\text{GAT}(\cdot)$  is a standard implementation of [32],  $H^L \in \mathbb{R}^{|L| \times d^g}$  is the learned representations as the output of the  $\text{GAT}_L$ .

To integrate location information into representation learning of activities and suppress the noise aggregated to the nodes of the activity layer, we introduce the localized-activity layer to pre-aggregate location embeddings. We first concatenate  $e_L$  and  $e_C$  to obtain the fused embedding matrix  $e_{LC} \in \mathbb{R}^{(|L|+|C|) \times d} = [e_L \ e_C]^\top$ . Then the localized-activity process is implemented as:

$$H^{LC'} = \text{GAT}_{LC}(e_{LC}, A^{LC'}), \quad (9)$$

where  $H^{LC'} \in \mathbb{R}^{(|L|+|C|) \times d^g}$  is the output of  $\text{GAT}_{LC}$ , we further slice out the first  $|L|$  rows of matrix  $H^{LC'}$  to obtain the pre-aggregated representation matrix  $H^{C'} \in \mathbb{R}^{|C| \times d^g}$ .

The learned representation  $H^{C'}$  is again concatenated with activity embeddings  $e_C$  as the  $\text{GAT}_C$ 's input  $e_{CC} = [e_C \ H^{C'}]^\top$ . It is worth noting that for all nodes in the activity layer, we could simultaneously aggregate information from neighbors in the localized-activity layer and neighbors in the same layer by simply modifying the matrix  $A^{CC'}$  to:

$$A_{new}^{CC'} = \begin{bmatrix} A^C & I_C \\ I_C & O_C \end{bmatrix}. \quad (10)$$

We still employ a similar strategy to update the representation of the nodes in the activity layer:

$$H^{C'} = \text{GAT}_C(e_{CC}, A_{new}^{CC'}), \quad (11)$$

where  $H^{C'} \in \mathbb{R}^{2|C| \times d^g}$  is the learned representation from  $\text{GAT}_C$ , we slice out the last  $|C|$  rows of matrix  $H^{C'}$  to obtain the updated activity node representation  $H^C \in \mathbb{R}^{|C| \times d^g}$ .

## Recurrent Encoder-Decoder Module

The *recurrent encoder-decoder module*'s structure is shown in Figure 4. Given a user  $u \in U$ 's history trajectory, the input of the activity and the location encoder at  $i$ th iteration are implemented as:

$$X_u^{C,i} = e_u \| e_{t_i} \| e_{c_i} \| H_{c_i}^C, \quad (12)$$

$$X_u^{L,i} = e_u \| e_{t_i} \| e_{l_i} \| H_{l_i}^C \| H_{l_i}^L, \quad (13)$$

where  $\|$  is the concatenation operation,  $H_{c_i}^C$  and  $H_{l_i}^L$  are the learned hierarchical graph representation of the activity node  $c_i$  and the location node  $l_i$ , the concatenated  $X_u^{C,i}$  and  $X_u^{L,i}$  are the inputs of the two encoders at the  $i$ th iteration.

Both activity and location encoders are implemented with LSTM, where hidden states updating process between  $h_u^{i,i}$  and  $h_u^{i,i-1}$  can be illustrated as:

$$p_u^i, f_u^i, g_u^i, o_u^i = \text{split}((W_x X_u^{i,i} + b_x) + (W_h h_u^{i,i-1} + b_h)), \quad (14)$$

$$c_u^{i,i} = \sigma(f_u^i) \odot c_u^{i,i-1} + \sigma(p_u^i) \odot \tanh(g_u^i), \quad (15)$$

$$h_u^{i,i} = \sigma(o_u^i) \odot \tanh(c_u^{i,i}), \quad (16)$$

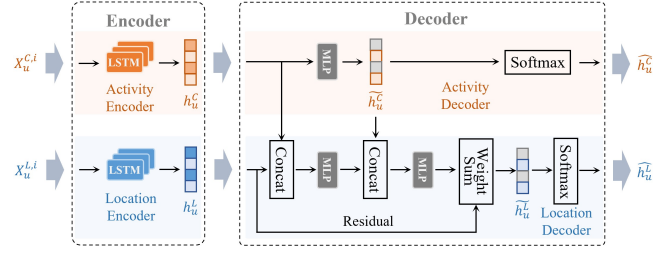


Figure 4: Recurrent encoder-decoder module's architecture.

where “ $\cdot$ ” can be either  $C$  or  $L$ .  $p_u^i, f_u^i, g_u^i, o_u^i$  are the input, forget, cell and output gates.  $c_u^{i,i}$  is the cell state at iteration  $i$ .  $\sigma(\cdot)$  and  $\tanh(\cdot)$  are the sigmoid and tanh activation functions.  $W_x, W_h, b_x$  and  $b_h$  are the trainable weights shared by inputs and  $\odot$  is the Hadamard product. Initial hidden states for  $h_u^{i,i}$  and  $c_u^{i,i}$  are set to zeros.

After obtaining final hidden states of activity and location encoder as  $h_u^C$  and  $h_u^L$ , we implement our activity decoder as a multi-layer perceptron (MLP) to get the next activity logits  $\widehat{h}_u^C \in \mathbb{R}^{|C|}$ :

$$\widehat{h}_u^C = \text{MLP}_C(h_u^C). \quad (17)$$

We finally residually combine the obtained activity logits with the encoded  $h_u^L$  to learn the location logits  $\widehat{h}_u^L \in \mathbb{R}^{|L|}$ :

$$\widehat{h}_u^L = \lambda_r \cdot \text{MLP}_L^r(h_u^L) + (1 - \lambda_r) \cdot \text{MLP}_L(\text{MLP}_L^h(h_u^L \| h_u^C) \| \widehat{h}_u^C), \quad (18)$$

where  $\lambda_r$  is a factor that controls the residual connections to trades off different features.

## HGARN Training

In this section we introduce the *model-agnostic history-enhanced confidence label* and explain the optimization process of HGARN.

*Model-Agnostic History-Enhanced Confidence Label Construction.* As human mobility trajectories exhibit repetitive nature (i.e., *recurring* mobility), existing models [8, 9] often try to capture periodicity by applying attention mechanisms to all user trajectories, have limited performances and interpretability. To overcome this, we modify the original label to get the *model-agnostic history-enhanced confidence label* (MAHEC label, in short), which can guide our model to focus on relevant user trajectories.

Specifically, for each location  $l^i \in L$ , we differentiate its confidence for a user  $u$ 's next location in two types:

$$\text{MAHEC}_{l^i}^u = \begin{cases} w^c, & \text{if } l^i = l_u^{|R_u|} \\ (1 - w^c) \cdot f_{l^i}^u, & \text{otherwise} \end{cases}, \quad (19)$$

$$f_{l^i}^u = \frac{1}{|R_u^{his}|} \sum_{l^i \in L} \mathbf{1}_{R_u^{his}}(l^i), \quad \mathbf{1}_{R_u^{his}}(l^i) = \begin{cases} 1, & \text{if } l^i \in R_u^{L, his} \\ 0, & \text{if } l^i \notin R_u^{L, his} \end{cases}, \quad (20)$$

where  $\mathbf{1}_{R_u^{his}}(\cdot)$  is an indicator function and  $w^c \in [0, 1]$  is a hyperparameter that indicates the confidence of the  $u$ 's ground truth label and  $f_{l^i}^u$  denotes the user  $u$ 's history visit frequency to  $l^i$ . Then the MAHEC label for the user  $u$ 's next location is as:

$$\text{MAHEC}_L^u = \left( \text{MAHEC}_{l^i}^u \right)_{i=1}^{|L|} \in \mathbb{R}^{|L|}, \quad (21)$$

where each element in  $\text{MAHEC}_L^u$  represents the confidence that the user  $u$  decides to pick as its next location. Similarly, we conduct the same operations for user activity trajectories to obtain  $\text{MAHEC}_C^u$ .

*Model Optimization.* Since next location prediction is a classification problem, we transform  $\widehat{h}_u^L$  to the probability distribution  $\widehat{h}_u^L \in \mathbb{R}^{|L|}$  of all locations by  $\widehat{h}_u^L = \text{Softmax}(\widehat{h}_u^L)$ . Given  $\text{MAHEC}_L^u$  and  $\widehat{h}_u^L$ , we compute  $\mathcal{L}_L$  based on cross-entropy loss:

$$\mathcal{L}_L = -\frac{1}{|U|} \sum_{u \in U} \sum_{i=1}^{|L|} \text{MAHEC}_L^u \cdot \log(\widehat{h}_u^{L,i}), \quad (22)$$

where  $\widehat{h}_u^{L,i}$  is the  $i$ th element of  $\widehat{h}_u^L$  and we compute the next activity loss  $\mathcal{L}_C$  based on same above described operations. Finally, we could train our HGARN end-to-end with a total loss function:

$$\mathcal{L} = \lambda_L \cdot \mathcal{L}_L + \lambda_C \cdot \mathcal{L}_C \quad (23)$$

$\lambda_L$  and  $\lambda_C$  are hyperparameters that trade off different loss terms.

## EXPERIMENTS

In this section, we compare our HGARN with existing SOTAs on two real-world LBSN check-in datasets.

### Datasets

**Table 1: Statistical information of NYC and TKY datasets.**

	user	activity	location	trajectory	ratio (Rec / Exp)
NYC	1065	308	4635	18918	85.9% / 14.1%
TKY	2280	286	7204	49039	91.5% / 8.5%

We adopt two LBSN datasets [38] containing Foursquare check-in records in New York City (NYC) and Tokyo (TKY) from April 12, 2012 to February 16, 2013, including 227,428 check-ins for NYC and 573,703 check-ins for TKY. The location distributions of NYC and TKY datasets are shown in Figure A1 in the appendix. Users and locations with less than 10 records are removed following previous work, and after cleaning, NYC and TKY have 308 and 286 activities, respectively. We divide the data into a training and testing sets in a ratio of 8:2, following the setting of [42]. Key data summary statistics are listed in Table 1.

### Baselines & Experimental Details

The following baseline methods are considered in experiments:

- **MC** [28]: MC is a widely used sequential prediction approach which models transition patterns based on visited locations.
- **STRNN** [21]: STRNN is an RNN-based model that incorporates the spatial-temporal contexts by leveraging transition matrices.
- **DEEPMOVE** [9]: DEEPMOVE uses attention mechanisms and an RNN module to capture users’ long- and short-term preferences.
- **LSTPM** [30]: LSTPM introduces a non-local network and a geo-dilated LSTM to model users’ long- and short-term preferences.
- **FLASHBACK** [36]: FLASHBACK is an RNN-based model that leverages spatial and temporal intervals to compute an aggregated hidden state from past hidden states for prediction.

- **PLSPL** [35]: PLSPL incorporates activity information to learn user preferences and utilizes two LSTMs to capture long-term and short-term preferences.
- **PG<sup>2</sup>NET** [16]: PG<sup>2</sup>NET learns users’ group and personalized preferences with spatial-temporal dependencies and attention-based Bi-LSTM.
- **GCDAN** [8]: GCDAN leverages graph convolution to learn spatial-temporal representations and use dual-attention to model the sequential dependencies.
- **CSLSL** [14]: CSLSL employs multi-task learning to model decision logic and two LSTMs to capture long- and short-term preferences.
- **GRAPH-FLASHBACK** [27]: GRAPH-FLASHBACK adds GCN to FLASHBACK to enrich learned transition graph representations constructed based on defined similarity functions over embeddings from the existing Knowledge Graph Embedding method.

For all baselines and our method, we adopt two commonly-employed metrics in prior works:  $\text{Rec}@K$  (Recall) and  $\text{NDCG}@K$  (Normalized Discounted Cumulative Gain). Specific formulas of

these two metrics are defined as:  $\text{Recall}@K = \frac{1}{|U|} \sum_{u \in U} \frac{|l_u^{R_u} \cap \widehat{l}_{u,K}^{R_u}|}{|\widehat{l}_{u,K}^{R_u}|}$

and  $\text{NDCG}@K = \frac{1}{|U|} \sum_{u \in U} \sum_{i=1}^K \frac{|l_u^{R_u} \cap \widehat{l}_{u,i}^{R_u}|}{\log(i+1)}$ , where  $\widehat{l}_{u,k}^{R_u}$  indicates the top  $k$  predicted locations.

We port all the baselines to our run time environment for fair comparisons based on their open-source codes. We carefully tuned their hyperparameters to get the best results. Additionally, unlike previous works that only evaluate overall model performances (under the main setting), we also conduct experiments under the *recurring* and *explorative* settings for more comprehensive performance evaluation against the existing SOTAs. For the main and *recurring* settings, we choose  $K = \{1, 5, 10\}$  for evaluation. As the performance is generally poorer under the *explorative* setting, we set  $K = \{10, 20\}$ .

For the choice of hyperparameters, we set both  $\lambda_L$  and  $\lambda_C$  to 1,  $\lambda_r$  to 0.6 for both datasets. For embedding dimensions, we set  $d = 200$ ,  $d^u = 10$ ,  $d^l = 30$ ,  $d^g = 50$  and the dimension of encoders’ hidden states are set to 600. Detailed reproducibility information can be found in supplementary materials.

## Main Results

Table 2 shows the main performance comparisons of different methods for the next location prediction. Our HGARN achieves state-of-the-art performances on all metrics for both datasets. Specifically, HGARN outperforms the best baseline approach by 12-19% on  $\text{Recall}@K$  and  $\text{NDCG}@K$  for NYC, and 11-20% for TKY. Its advantages become more significant as  $K$  increases, validating the effectiveness of the hierarchical graph modeling and MAHEC label for the next location prediction task.

In addition, we also evaluate different models separately in the *recurring* and *explorative* settings. In the *recurring* setting, based on results in Table 3, our model shows an improvement of (10.8%, 23.4%, 31.6%, 10.8%, 19.1%, 20.1%) and (9.4%, 19.2%, 19.7%, 9.4%, 16.5%, 16.9%) on all metrics ( $\text{R}@1$ ,  $\text{R}@5$ ,  $\text{R}@10$ ,  $\text{N}@1$ ,  $\text{N}@5$ ,  $\text{N}@10$ ) compared to the best baseline on the two datasets. HGARN outperforms all baselines significantly in the *recurring* setting.

Table 2: Main performance comparisons of different methods in two real-world datasets.

Main	NYC						TKY					
	R@1	R@5	R@10	N@1	N@5	N@10	R@1	R@5	R@10	N@1	N@5	N@10
Mc	0.189	0.364	0.407	0.189	0.284	0.298	0.170	0.313	0.347	0.170	0.247	0.258
STRNN	0.162	0.255	0.287	0.162	0.213	0.223	0.123	0.209	0.246	0.123	0.169	0.180
DEEPMOVE	0.243	0.387	0.413	0.243	0.322	0.331	0.166	0.268	0.307	0.166	0.221	0.233
LSTPM	0.235	0.436	0.492	0.235	0.342	0.361	0.205	0.366	0.416	0.205	0.292	0.309
FLASHBACK	0.219	0.368	0.423	0.219	0.299	0.317	0.209	0.387	0.447	0.209	0.305	0.325
PG <sup>2</sup> NET	0.206	0.400	0.430	0.206	0.313	0.323	0.197	0.333	0.376	0.197	0.270	0.284
PLSPL	0.187	0.315	0.365	0.187	0.258	0.274	0.166	0.272	0.315	0.166	0.222	0.236
GCDAN	0.188	0.311	0.344	0.188	0.256	0.267	0.171	0.297	0.343	0.171	0.239	0.253
CSSL	0.231	0.387	0.421	0.231	0.317	0.328	0.210	0.367	0.417	0.210	0.294	0.310
G-FLASHBACK	0.219	0.371	0.428	0.219	0.300	0.319	0.209	0.387	0.441	0.209	0.304	0.322
HGARN (our)	<b>0.273</b>	<b>0.520</b>	<b>0.575</b>	<b>0.273</b>	<b>0.405</b>	<b>0.423</b>	<b>0.234</b>	<b>0.461</b>	<b>0.526</b>	<b>0.234</b>	<b>0.355</b>	<b>0.376</b>

Table 3: Results under the *recurring* setting.

Recurring	NYC						TKY					
	R@1	R@5	R@10	N@1	N@5	N@10	R@1	R@5	R@10	N@1	N@5	N@10
Mc	0.237	0.430	0.474	0.237	0.342	0.357	0.199	0.371	0.408	0.199	0.292	0.304
STRNN	0.189	0.248	0.259	0.189	0.248	0.259	0.162	0.273	0.316	0.162	0.221	0.235
DEEPMOVE	0.243	0.387	0.413	0.243	0.322	0.331	0.209	0.332	0.372	0.209	0.275	0.288
LSTPM	0.282	0.513	0.533	0.282	0.409	0.428	0.249	0.433	0.484	0.249	0.348	0.364
FLASHBACK	0.283	0.507	0.554	0.283	0.406	0.422	0.250	0.462	0.527	0.250	0.363	0.384
PG <sup>2</sup> NET	0.285	0.492	0.526	0.285	0.398	0.409	0.252	0.411	0.459	0.252	0.338	0.354
PLSPL	0.251	0.413	0.450	0.251	0.340	0.352	0.209	0.336	0.384	0.209	0.277	0.292
GCDAN	0.242	0.405	0.439	0.242	0.331	0.342	0.227	0.389	0.436	0.227	0.315	0.330
CSSL	0.288	0.498	0.542	0.288	0.404	0.418	0.254	0.457	0.511	0.254	0.364	0.382
G-FLASHBACK	0.282	0.509	0.562	0.282	0.406	0.423	0.252	0.463	0.527	0.252	0.364	0.385
HGARN (our)	<b>0.319</b>	<b>0.633</b>	<b>0.713</b>	<b>0.319</b>	<b>0.487</b>	<b>0.514</b>	<b>0.278</b>	<b>0.552</b>	<b>0.631</b>	<b>0.278</b>	<b>0.424</b>	<b>0.450</b>

Table 4: Results under the *explorative* setting.

Explorative	NYC				TKY			
	R@10	R@20	N@10	N@20	R@10	R@20	N@10	N@20
STRNN	0.066	0.071	0.031	0.033	0.047	0.064	0.021	0.026
DEEPMOVE	0.064	0.112	0.036	0.049	0.04	0.051	0.020	0.031
LSTPM	0.091	0.115	0.052	0.058	0.067	0.090	<b>0.041</b>	<b>0.047</b>
FLASHBACK	0.083	0.109	0.045	0.051	0.053	0.072	0.028	0.032
PG <sup>2</sup> NET	0.046	0.054	0.021	0.023	0.056	0.065	0.029	0.032
PLSPL	0.051	0.061	0.029	0.032	0.056	0.065	0.026	0.032
GCDAN	0.049	0.056	0.025	0.027	0.036	0.048	0.020	0.023
CSSL	0.078	0.115	0.048	0.057	0.062	0.095	0.030	0.038
GRAPH-FLASHBACK	0.078	0.104	0.044	0.051	0.053	0.072	0.028	0.032
HGARN (our)	<b>0.102</b>	<b>0.135</b>	<b>0.054</b>	<b>0.062</b>	<b>0.081</b>	<b>0.120</b>	0.037	<b>0.047</b>

As shown in Table 4<sup>2</sup>, the overall results in the *explorative* setting are much lower than those in the main and *recurring* settings, which is intuitive because of the inherent difficulty of predicting unseen locations. A possible approach to improving the prediction in the *explorative* setting is to model the dependencies between locations. In addition, due to the larger number of locations in the TKY dataset, the hierarchical graph modeling may introduce noise, making our model less effective in ranking the predicted locations. The above hypotheses may also be why our model performs better in Recall but are not consistently better in NDCG.

## Ablation Study

To study each component of HGARN, we conduct an ablation study considering the following four variants of HGARN: (1) HGARN w/o HGAT contains only the *recurrent encoder-decoder module* for the

<sup>2</sup>The Mc’s results are all zeros and thus deleted from the table.

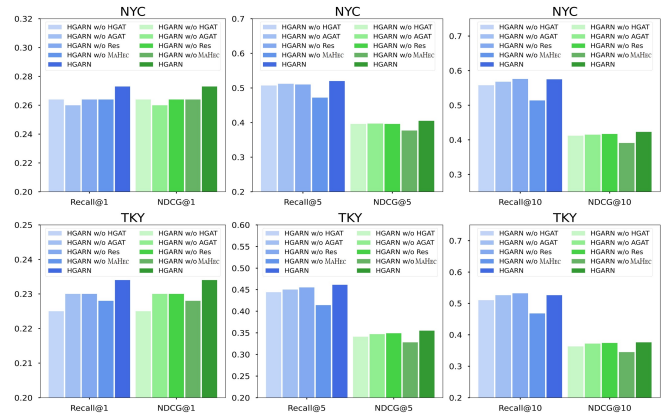


Figure 5: Ablation study results visualization.

next location prediction. (2) HGARN w/o AGAT: This variant’s *hierarchical graph attention module* contains only the location layer and corresponding graph attention networks. (3) HGARN w/o Res is the variant that removes the residual connection of the *recurrent encoder-decoder module*. (4) HGARN w/o MAHEC is the variant that leverages original labels to optimize our model. The ablation study results are shown in Figure 5. It is found that all metrics get improved as more components are included. The gradual increase in prediction results from HGARN w/o HGAT to HGARN w/o AGAT to HGARN is a fine-grained demonstration of the effectiveness of GAT in each layer of the hierarchical graph. In addition, the model’s performance improvements by adding the MAHEC label is significant when  $K$  are large, verifying its effectiveness under simplicity.

## Hyperparameter Sensitivity Analysis

We further study the sensitivity of a few key parameters by varying each parameter while keeping others constant. (1)  $D^h$  affects the location dependencies, too high or too low will lead to decreased performances. The best results were obtained at  $D^h = 1\text{km}$  on NYC and optimal at  $D^h = 0.1\text{km}$  on TKY, this is probably because the geographic space and the distance between locations are larger in NYC than in TKY, as in Figure A1. (2)  $w^c$  A affects the model’s attention to history locations. The results show an upward and

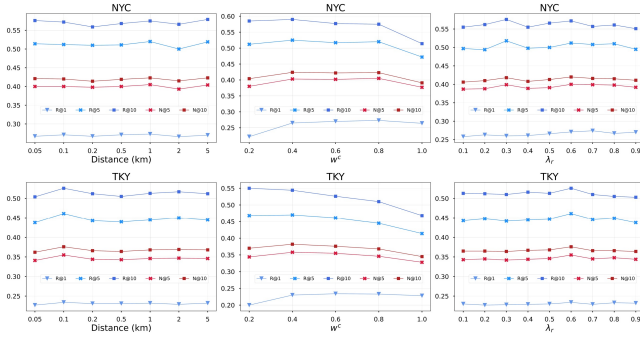


Figure 6: Sensitivity experiments results on two datasets.

then downward trend as  $w^c$  rises on both datasets, indicating that both too large and too small dependence on locations in the history trajectory is detrimental to the model’s performance. (3)  $\lambda_r$  affects how much activity information is fused in predicting the next location. Intuitively, a  $\lambda_r$  too high would introduce noise, and too low may result in ineffective utilization of activity information. The results align with our conjecture that the model achieves optimal performance with  $\lambda_r$  at 0.6 for both NYC and TKY datasets.

### Interpretability Analysis

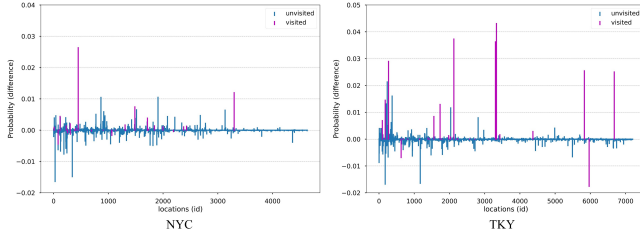


Figure 7: The predicted locations probability distributions difference (with MAHEC minus without MAHEC) of two randomly selected human trajectories on two datasets.

*How does MAHEC labels work?* To understand the mechanism of MAHEC label, we randomly selected two human trajectories from two datasets and visualized the predicted probability difference of “HGARN” and “HGARN w/o MAHEC”. Figure 7 shows the probability change, where the purple line represents the locations in the current user’s history trajectory. With MAHEC labels, the probability distribution of the next location predicted by the model increases in most of the visited locations, demonstrating that our MAHEC labels can effectively guide the model to pay attention to the user’s history trajectory when predicting the next location. The mechanism of MAHEC can also interpret, to some extent, why the prediction performances of our HGARN can far exceed that of the baseline methods, especially under the *recurring* setting.

*What the Hierarchical Graph learned?* Unlike other methods that have difficulty interpreting learned higher-order spatial-temporal dependencies, our HGARN can somewhat understand the dependencies between activities through the learned Hierarchical Graph.

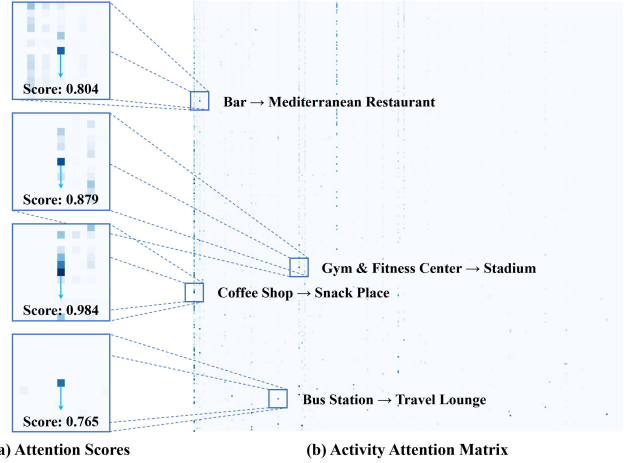


Figure 8: A visualization of activities attentions and cases.

We visualize one attention head of  $GAT_C$ ’s sliced attention matrix to analyze the learned activity-activity dependencies. In Figure 8, We select four activity pairs to show the related activities and their corresponding attention scores. These activity pairs are intuitive and consistent with common sense human travel, such as the high dependencies between Gyms and Stadiums, Bus Stops and Travel Lounges. These results have important implications for understanding human activity patterns and predicting the next location.

### CONCLUSION

Both travel behavior theories and empirical evidence suggest that human mobility patterns largely depend on the need to participate in activities at different times of the day. Therefore, it is crucial to consider the latter when modeling the former. In this paper, we propose a *Hierarchical Graph Attention Recurrent Network* (HGARN) for activity-aware human mobility prediction. Specifically, HGARN introduces hierarchical graph attention mechanisms on a constructed hierarchical graph to model time-activity-location dependencies, and employ next activity prediction as an auxiliary task to further improve the main task of the next location prediction. In addition, we propose a simple yet powerful MAHEC label that can guide our model to flexibly tradeoff the importance of history locations when predicting future locations. Finally, we perform comprehensive experiments to demonstrate the superiority of HGARN, this is the first work to evaluate existing models and our HGARN under *recurring* and *explorative* settings to our best knowledge. We find that introducing activity information can effectively improve the model’s prediction accuracy. In addition, our results show that the existing models have unsatisfactory prediction performances under the *explorative* setting. We hope our work could spark the attention of future work on *explorative* mobility prediction. For future work, we consider adding a ranking-based component to organize high-probability candidate locations and incorporate human travel decision logic modeling to make more interpretable predictions.



## REFERENCES

- [1] Jie Bao, Yu Zheng, and Mohamed F Mokbel. 2012. Location-based and preference-aware recommendation using sparse geo-social networking data. In *Proceedings of the 20th international conference on advances in geographic information systems*. 199–208.
- [2] Joe Castiglione, Mark Bradley, and John Gliebe. 2015. *Activity-based travel demand models: a primer*. Number SHRP 2 Report S2-C46-RR-1.
- [3] Buru Chang, Gwanghoon Jang, Seoyoon Kim, and Jaewoo Kang. 2020. Learning graph-based geographical latent representation for point-of-interest recommendation. In *Proceedings of the 29th ACM International Conference on Information & Knowledge Management*. 135–144.
- [4] Buru Chang, Yonggyu Park, Donghyeon Park, Seongsoon Kim, and Jaewoo Kang. 2018. Content-aware hierarchical point-of-interest embedding model for successive poi recommendation. In *IJCAI*, Vol. 2018. 27th.
- [5] Chen Cheng, Haiqin Yang, Michael R Lyu, and Irwin King. 2013. Where you like to go next: Successive point-of-interest recommendation. In *Twenty-Third international joint conference on Artificial Intelligence*.
- [6] Kyunghyun Cho, Bart Van Merriënboer, Caglar Gulcehre, Dzmitry Bahdanau, Fethi Bougares, Holger Schwenk, and Yoshua Bengio. 2014. Learning phrase representations using RNN encoder-decoder for statistical machine translation. *arXiv preprint arXiv:1406.1078* (2014).
- [7] Junyoung Chung, Caglar Gulcehre, KyungHyun Cho, and Yoshua Bengio. 2014. Empirical evaluation of gated recurrent neural networks on sequence modeling. *arXiv preprint arXiv:1412.3555* (2014).
- [8] Weizhen Dang, Haibo Wang, Shirui Pan, Pei Zhang, Chuan Zhou, Xin Chen, and Jilong Wang. 2022. Predicting Human Mobility via Graph Convolutional Dual-attentive Networks. In *Proceedings of the Fifteenth ACM International Conference on Web Search and Data Mining*. 192–200.
- [9] Jie Feng, Yong Li, Chao Zhang, Funing Sun, Fanchao Meng, Ang Guo, and Depeng Jin. 2018. Deepmove: Predicting human mobility with attentional recurrent networks. In *Proceedings of the 2018 world wide web conference*. 1459–1468.
- [10] Sébastien Gambs, Marc-Olivier Killijian, and Miguel Núñez del Prado Cortez. 2012. Next place prediction using mobility markov chains. In *Proceedings of the first workshop on measurement, privacy, and mobility*. 1–6.
- [11] Kan Guo, Yongli Hu, Yanfeng Sun, Sean Qian, Junbin Gao, and Baocai Yin. 2021. Hierarchical Graph Convolution Network for Traffic Forecasting. In *Proceedings of the AAAI Conference on Artificial Intelligence*, Vol. 35. 151–159.
- [12] Qing Guo, Zhu Sun, Jie Zhang, and Yin-Leng Theng. 2020. An attentional recurrent neural network for personalized next location recommendation. In *Proceedings of the AAAI Conference on artificial intelligence*, Vol. 34. 83–90.
- [13] Sepp Hochreiter and Jürgen Schmidhuber. 1997. Long short-term memory. *Neural computation* 9, 8 (1997), 1735–1780.
- [14] Zongyuan Huang, Shengyuan Xu, Menghan Wang, Hansi Wu, Yanyan Xu, and Yaohui Jin. 2022. Human Mobility Prediction with Causal and Spatial-constrained Multi-task Network. *arXiv preprint arXiv:2206.05731* (2022).
- [15] Thomas N Kipf and Max Welling. 2016. Semi-supervised classification with graph convolutional networks. *arXiv preprint arXiv:1609.02907* (2016).
- [16] Huifeng Li, Bin Wang, Fan Xia, Xi Zhai, Sulei Zhu, and Yanyan Xu. 2021. PG<sup>2</sup>Net: Personalized and Group Preferences Guided Network for Next Place Prediction. *arXiv preprint arXiv:2110.08266* (2021).
- [17] Ranzhen Li, Yanyan Shen, and Yanmin Zhu. 2018. Next point-of-interest recommendation with temporal and multi-level context attention. In *2018 IEEE International Conference on Data Mining (ICDM)*. IEEE, 1110–1115.
- [18] Defu Lian, Yongji Wu, Yong Ge, Xing Xie, and Enhong Chen. 2020. Geography-aware sequential location recommendation. In *Proceedings of the 26th ACM SIGKDD international conference on knowledge discovery & data mining*. 2009–2019.
- [19] Nicholas Lim, Bryan Hooi, See-Kiong Ng, Yong Liang Goh, Renrong Weng, and Rui Tan. 2022. Hierarchical Multi-Task Graph Recurrent Network for Next POI Recommendation. (2022).
- [20] Nicholas Lim, Bryan Hooi, See-Kiong Ng, Xueou Wang, Yong Liang Goh, Renrong Weng, and Jagannadan Varadarajan. 2020. STP-UDGAT: spatial-temporal-preference user dimensional graph attention network for next POI recommendation. In *Proceedings of the 29th ACM International Conference on Information & Knowledge Management*. 845–854.
- [21] Qiang Liu, Shu Wu, Liang Wang, and Tieniu Tan. 2016. Predicting the next location: A recurrent model with spatial and temporal contexts. In *Thirtieth AAAI conference on artificial intelligence*.
- [22] Yingtao Luo, Qiang Liu, and Zhaocheng Liu. 2021. Stan: Spatio-temporal attention network for next location recommendation. In *Proceedings of the Web Conference 2021*. 2177–2185.
- [23] Qingsong Lv, Ming Ding, Qiang Liu, Yuxiang Chen, Wenzheng Feng, Siming He, Chang Zhou, Jianguo Jiang, Yuxiao Dong, and Jie Tang. 2021. Are we really making much progress? Revisiting, benchmarking and refining heterogeneous graph neural networks. In *Proceedings of the 27th ACM SIGKDD Conference on Knowledge Discovery & Data Mining*. 1150–1160.
- [24] Jarana Manotumruksa, Craig Macdonald, and Iadh Ounis. 2017. A deep recurrent collaborative filtering framework for venue recommendation. In *Proceedings of the 2017 ACM on Conference on Information and Knowledge Management*. 1429–1438.
- [25] Baichuan Mo, Zhan Zhao, Haris N Koutsopoulos, and Jinhua Zhao. 2021. Individual mobility prediction in mass transit systems using smart card data: an interpretable Activity-based hidden Markov approach. *IEEE Transactions on Intelligent Transportation Systems* (2021).
- [26] Luca Pappalardo, Filippo Simini, Salvatore Rinzivillo, Dino Pedreschi, Fosca Giannotti, and Albert-László Barabási. 2015. Returners and explorers dichotomy in human mobility. *Nature communications* 6, 1 (2015), 1–8.
- [27] Xuan Rao, Lisi Chen, Yong Liu, Shuo Shang, Bin Yao, and Peng Han. 2022. Graph-Flashback Network for Next Location Recommendation. In *Proceedings of the 28th ACM SIGKDD Conference on Knowledge Discovery and Data Mining*. 1463–1471.
- [28] Steffen Rendle, Christoph Freudenthaler, and Lars Schmidt-Thieme. 2010. Factorizing personalized markov chains for next-basket recommendation. In *Proceedings of the 19th international conference on World wide web*. 811–820.
- [29] Markus Schläpfer, Lei Dong, Kevin O’Keeffe, Paolo Santi, Michael Szell, Hadrien Salat, Samuel Ankesaria, Mohammad Vazifeh, Carlo Ratti, and Geoffrey B West. 2021. The universal visitation law of human mobility. *Nature* 593, 7860 (2021), 522–527.
- [30] Ke Sun, Tiejun Qian, Tong Chen, Yile Liang, Quoc Viet Hung Nguyen, and Hongzhi Yin. 2020. Where to go next: Modeling long-and short-term user preferences for point-of-interest recommendation. In *Proceedings of the AAAI Conference on Artificial Intelligence*, Vol. 34. 214–221.
- [31] Ashish Vaswani, Noam Shazeer, Niki Parmar, Jakob Uszkoreit, Llion Jones, Aidan N Gomez, Łukasz Kaiser, and Illia Polosukhin. 2017. Attention is all you need. *Advances in neural information processing systems* 30 (2017).
- [32] Petar Veličković, Guillem Cucurull, Arantxa Casanova, Adriana Romero, Pietro Lio, and Yoshua Bengio. 2017. Graph attention networks. *arXiv preprint arXiv:1710.10903* (2017).
- [33] Huangdong Wang, Qiaohong Yu, Yu Liu, Depeng Jin, and Yong Li. 2021. Spatio-Temporal Urban Knowledge Graph Enabled Mobility Prediction. *Proceedings of the ACM on Interactive, Mobile, Wearable and Ubiquitous Technologies* 5, 4 (2021), 1–24.
- [34] Ning Wu, Xin Wayne Zhao, Jingyuan Wang, and Dayan Pan. 2020. Learning effective road network representation with hierarchical graph neural networks. In *Proceedings of the 26th ACM SIGKDD International Conference on Knowledge Discovery & Data Mining*. 6–14.
- [35] Yuxia Wu, Ke Li, Guoshuai Zhao, and QIAN Xueming. 2020. Personalized long-and short-term preference learning for next POI recommendation. *IEEE Transactions on Knowledge and Data Engineering* (2020).
- [36] Dingqi Yang, Benjamin Fankhauser, Paolo Rosso, and Philippe Cudre-Mauroux. 2020. Location Prediction over Sparse User Mobility Traces Using RNNs. In *Proceedings of the Twenty-Ninth International Joint Conference on Artificial Intelligence*. 2184–2190.
- [37] Dingqi Yang, Bingqing Qu, Jie Yang, and Philippe Cudre-Mauroux. 2019. Revisiting user mobility and social relationships in lbsns: a hypergraph embedding approach. In *The world wide web conference*. 2147–2157.
- [38] Dingqi Yang, Daqing Zhang, Vincent W Zheng, and Zhiyong Yu. 2014. Modeling user activity preference by leveraging user spatial temporal characteristics in LBSNs. *IEEE Transactions on Systems, Man, and Cybernetics: Systems* 45, 1 (2014), 129–142.
- [39] Fuqiang Yu, Lizhen Cui, Wei Guo, Xudong Lu, Qingzhong Li, and Hua Lu. 2020. A category-aware deep model for successive POI recommendation on sparse check-in data. In *Proceedings of the web conference 2020*. 1264–1274.
- [40] Jia-Dong Zhang, Chi-Yin Chow, and Yanhua Li. 2014. Lore: Exploiting sequential influence for location recommendations. In *Proceedings of the 22nd ACM SIGSPATIAL International Conference on Advances in Geographic Information Systems*. 103–112.
- [41] Weijia Zhang, Hao Liu, Yanchi Liu, Jingbo Zhou, and Hui Xiong. 2020. Semi-supervised hierarchical recurrent graph neural network for city-wide parking availability prediction. In *Proceedings of the AAAI Conference on Artificial Intelligence*, Vol. 34. 1186–1193.
- [42] Pengpeng Zhao, Anjing Luo, Yanchi Liu, Fuzhen Zhuang, Jiajie Xu, Zhixu Li, Victor S Sheng, and Xiaofang Zhou. 2020. Where to go next: A spatio-temporal gated network for next poi recommendation. *IEEE Transactions on Knowledge and Data Engineering* (2020).
- [43] Zhan Zhao, Haris N. Koutsopoulos, and Jinhua Zhao. 2018. Individual mobility prediction using transit smart card data. *Transportation Research Part C: Emerging Technologies* 89 (April 2018), 19–34. <https://doi.org/10.1016/j.trc.2018.01.022>
- [44] Dingyi Zhuang, Shenhao Wang, Haris Koutsopoulos, and Jinhua Zhao. 2022. Uncertainty Quantification of Sparse Travel Demand Prediction with Spatial-Temporal Graph Neural Networks. In *Proceedings of the 28th ACM SIGKDD Conference on Knowledge Discovery and Data Mining*. 4639–4647.

## APPENDIX

In this section, we provide more details, visualizations and experimental results.

### Experimental Supplementary

Figure A1 demonstrated the location distribution of NYC and TKY datasets.

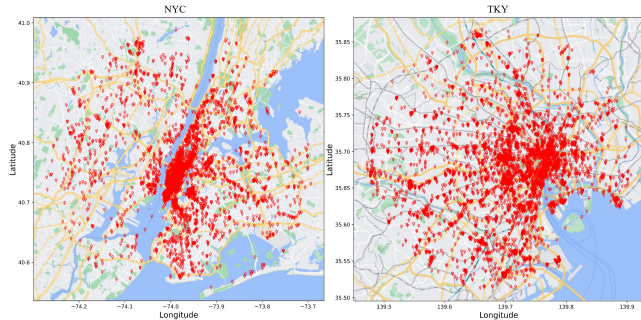


Figure A1: Location distributions of NYC and TKY.

Figure A2 displayed two more probability distribution change cases with the effect of MAHeC labels.

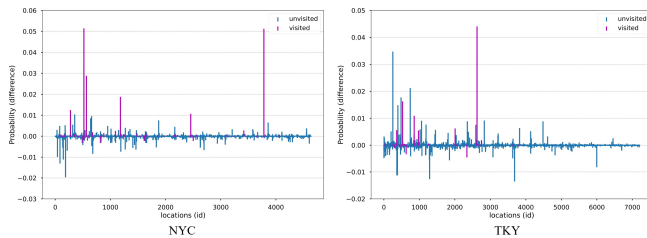


Figure A2: More visualizations of predicted locations probability distributions on two datasets.

### Introduction’s supplementary

Given the recent emphasis on modeling contextual information (e.g., spatio-temporal) in mobility prediction approaches, we find little work analyzing changes in model prediction performances other than adding or removing relevant components (i.e., ablation studies) and parameter sensitivities. However, it is well-known that human mobility exhibits two different tendencies, i.e., returning to "old" places and exploring "new" ones [26]. Inspired by this dichotomy, we can define *recurring* and *explorative* mobility based on whether a user’s next location is seen before, as illustrated in Figure A3. Human mobility trajectories contain both *recurring* and *explorative* tendencies, although different users may have different mixtures of the two. When data is sparse, the latter may seem more pronounced, exacerbating the challenge of the next location prediction. Therefore, when evaluating those mobility prediction models, it is necessary to assess their predictive power under both *recurring* and *explorative* settings in addition to the main setting.

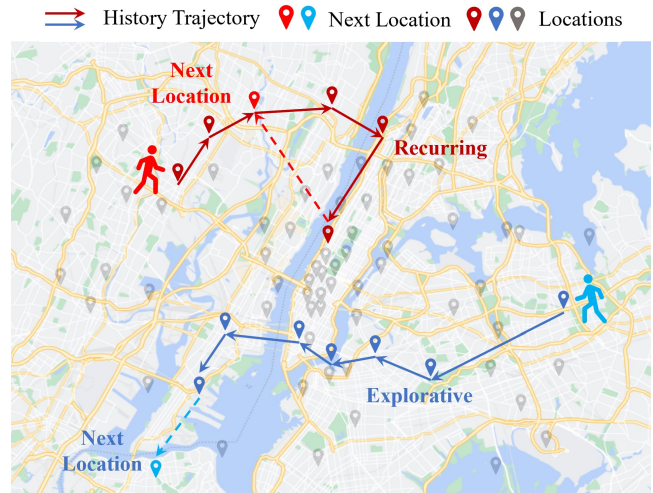


Figure A3: An illustration of *Recurring* and *Explorative* mobility. Given a user’s history trajectory, *Recurring* mobility indicates a user’s next location is a visited one. In contrast, *Explorative* mobility is more unpredictable, indicating a user’s next location was not visited in the history mobility.

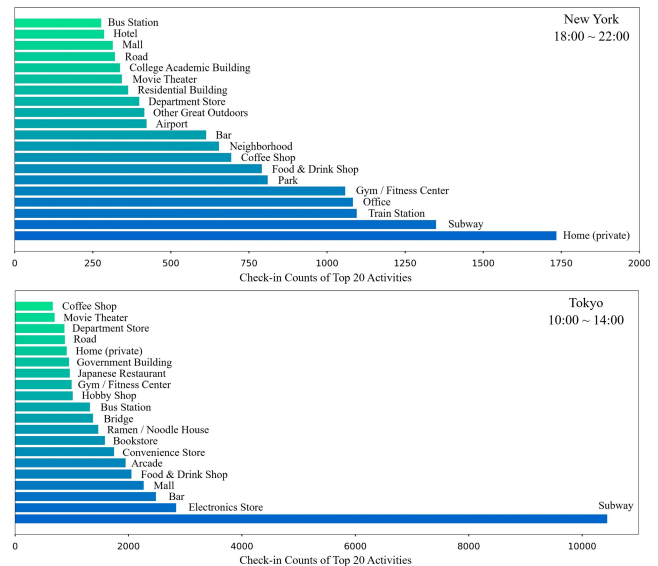


Figure A4: Activity distribution statistics in New York and Tokyo at two different time periods.

Figure A4 demonstrated a strong temporal dependency between activities, and we remove TKY’s top-1 activity Train Station for better visualization.

### Reproducibility

In this section, to address the reproducibility of our experiments, we provide the specific information about computing devices and detailed hyperparameter settings used in our experiments.

All models (our HGARN and other baselines) with learnable parameters are trained on a desktop with Intel Core i9-10990K CPU @3.7GHz  $\times$  10, 2666MHz  $\times$  2  $\times$  16GB RAM, GeForce RTX 3080  $\times$  2, 500GB SSD. We implement HGARN based on Pytorch. Parameters of HGARN are randomly initialized and optimized by the Adam optimizer with a learning rate of 2e-4, decaying by 0.8 with each epoch and we train HGARN by 80 epochs.

For hyperparameter settings, we set  $\lambda_L = \lambda_C = 1$ , and dimensions  $d^g = 50$ ,  $d = 200$ ,  $d^u = 20$ ,  $d^t = 30$ . Location and activity encoders have hidden states with dimensions of 600. The above settings remain the same in all experiment settings. For the main and *recurring* settings of all datasets, we employ 2 attention heads and set the dropout to 0.1, while for the *explorative* setting of all datasets, we let the number of attention heads be 1 and set the dropout to 0.6 to prevent overfitting. For the NYC main and *recurring* settings, we set  $D^h$  to 1,  $w^c$  to 0.8, and  $\lambda_r$  to 0.6, while for the *explorative* setting,  $D^h$ ,  $w^c$ , and  $\lambda_r$  is set to 0.1, 0.9, and 1, respectively. for the TKY main and *recurring* settings,  $D^h$ ,  $w^c$ , and  $\lambda_r$  are set to 0.1, 0.6 and 0.6 for TKY’s main and *recurring*, respectively, and 0.1, 1, 0.5 for the *explorative* setting. (All notations mentioned above, their corresponding explanations could be found in the main text)

## Full Numerical Results

In this section, we show the complete numerical results for the figures presented in the main part. Table A2 contains complete numerical results for  $D^h$ ’s sensitivity experiments. Table A3 contains complete numerical results for  $\lambda_r$ ’s sensitivity experiments. Table A1 contains complete numerical results for  $w^c$ ’s sensitivity experiments. Table A4 contains complete numerical results for our ablation study. Detailed analysis of the relevant experimental results can be found in the experimental section of the main part.

**Table A1: Full results of  $w^c$ ’s sensitivity experiments.**

$w^c$ (MAHEC)		0.2	0.4	0.6	0.8	1.0
NYC	R@1	0.222	0.265	0.270	0.273	0.264
	R@5	0.512	0.525	0.517	0.520	0.472
	R@10	0.585	0.590	0.577	0.575	0.514
	N@1	0.222	0.265	0.270	0.273	0.264
	N@5	0.380	0.403	0.402	0.405	0.377
	N@10	0.404	0.424	0.422	0.423	0.391
TKY	R@1	0.200	0.230	0.234	0.233	0.228
	R@5	0.468	0.470	0.461	0.445	0.414
	R@10	0.550	0.544	0.526	0.510	0.468
	N@1	0.200	0.230	0.234	0.233	0.228
	N@5	0.344	0.358	0.355	0.346	0.328
	N@10	0.370	0.382	0.376	0.368	0.345

**Table A2: Full results of  $D^h$ ’s sensitivity experiments.**

$D^h$		0.05	0.1	0.2	0.5	1	2	5
NYC	R@1	0.267	0.271	0.267	0.271	0.273	0.266	0.270
	R@5	0.514	0.512	0.510	0.511	0.520	0.500	0.519
	R@10	0.576	0.572	0.559	0.568	0.575	0.566	0.579
	N@1	0.267	0.271	0.267	0.271	0.273	0.266	0.270
	N@5	0.400	0.400	0.398	0.400	0.405	0.393	0.404
	N@10	0.421	0.420	0.414	0.419	0.423	0.415	0.423
TKY	R@1	0.227	0.234	0.231	0.231	0.232	0.229	0.232
	R@5	0.438	0.461	0.443	0.440	0.445	0.450	0.445
	R@10	0.504	0.526	0.512	0.505	0.513	0.517	0.512
	N@1	0.227	0.234	0.231	0.231	0.232	0.229	0.232
	N@5	0.341	0.355	0.344	0.343	0.346	0.347	0.346
	N@10	0.362	0.376	0.366	0.364	0.368	0.369	0.368

**Table A3: Full results of  $\lambda_r$ ’s sensitivity experiments.**

$\lambda_r$		0.1	0.2	0.3	0.4	0.5	0.6	0.7	0.8	0.9
NYC	R@1	0.258	0.263	0.260	0.261	0.266	0.271	0.274	0.267	0.270
	R@5	0.497	0.494	0.518	0.498	0.500	0.512	0.508	0.510	0.495
	R@10	0.555	0.562	0.576	0.555	0.566	0.572	0.557	0.561	0.551
	N@1	0.258	0.263	0.260	0.261	0.266	0.271	0.274	0.267	0.270
	N@5	0.387	0.388	0.399	0.389	0.391	0.400	0.399	0.398	0.392
	N@10	0.406	0.410	0.418	0.408	0.413	0.420	0.416	0.415	0.411
TKY	R@1	0.230	0.227	0.228	0.229	0.230	0.234	0.229	0.233	0.232
	R@5	0.443	0.448	0.442	0.445	0.447	0.461	0.446	0.449	0.438
	R@10	0.513	0.512	0.510	0.516	0.513	0.526	0.510	0.505	0.503
	N@1	0.230	0.227	0.228	0.229	0.230	0.234	0.229	0.233	0.232
	N@5	0.343	0.345	0.342	0.344	0.346	0.355	0.345	0.348	0.344
	N@10	0.365	0.365	0.364	0.367	0.368	0.376	0.366	0.366	0.364

**Table A4: Full results of the ablation study.**

Ablations		w/o HGAT	w/o AGAT	w/o RES	w/o MAHEC	HGARN
NYC	R@1	0.264	0.260	0.264	0.264	0.273
	R@5	0.507	0.512	0.510	0.472	0.520
	R@10	0.558	0.568	0.576	0.514	0.575
	N@1	0.264	0.260	0.264	0.264	0.273
	N@5	0.396	0.397	0.396	0.377	0.405
	N@10	0.412	0.415	0.417	0.391	0.423
TKY	R@1	0.225	0.230	0.230	0.228	0.234
	R@5	0.444	0.450	0.455	0.414	0.461
	R@10	0.510	0.526	0.532	0.468	0.526
	N@1	0.225	0.230	0.230	0.228	0.234
	N@5	0.341	0.347	0.349	0.328	0.355
	N@10	0.363	0.372	0.374	0.345	0.376